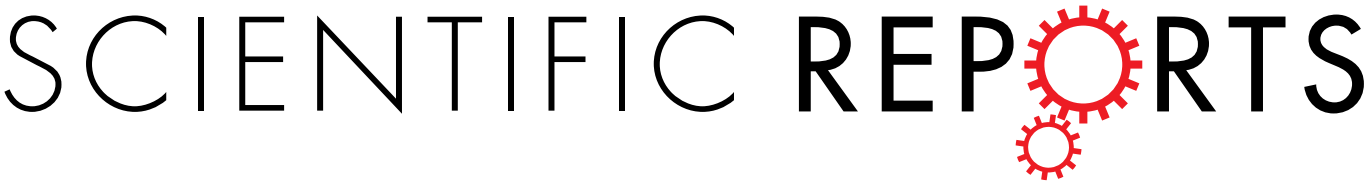

OPEN

Understanding of MoS_2/GaN Heterojunction Diode and its Photodetection Properties

Received: 30 April 2018
Accepted: 11 July 2018
Published online: 07 August 2018

Monika Moun, Mukesh Kumar, Manjari Garg, Ravi Pathak & Rajendra Singh

Fabrication of heterojunction between 2D molybdenum disulfide (MoS_2) and gallium nitride (GaN) and its photodetection properties have been reported in the present work. Surface potential mapping at the MoS_2/GaN heterojunction is done using Kelvin Probe Force Microscopy to measure the conduction band offset. Current-voltage measurements show a diode like behavior of the heterojunction. The origin of diode like behavior is attributed to unique type II band alignment of the heterojunction. The photocurrent, photoresponsivity and detectivity of the heterojunction are found to be dependent on power density of the light. Photoresponse investigations reveal that the heterojunction is highly sensitive to 405 nm laser with very high responsivity up to 10^5 A/W. The heterojunction also shows very high detectivity of the order of 10^{14} Jones. Moreover, the device shows photoresponse in UV region also. These observations suggest that MoS_2/GaN heterojunction can have great potential for photodetection applications.

Two dimensional transition metal dichalcogenides (TMDCs) have garnered a great research interest due to their unique electrical, mechanical, optical and chemical properties making them preferable for potential applications in electronic and optoelectronic devices[1–3]. Weak interlayer van der Waals interaction present in TMDCs facilitates the exfoliation of bulk crystal in few layers offering layer dependent unique properties[4,5]. Since most of the 2D materials have relatively smaller bandgap, optoelectronic and photovoltaic devices based on these semiconductors can be realized due to their excellent light absorption properties[6–8]. Molybdenum disulfide (MoS_2) is a typical layered transition metal dichalcogenide having indirect bandgap of 1.2 eV in bulk form and direct bandgap of 1.8 eV when it is in monolayer form[4,9]. Due to its unique layer dependent appealing properties such as high mobility and excellent light absorption covering broad range of spectral response, it has been extensively studied by scientists for various applications such as field effect transistors[10,11], gas sensors[12,13], photodetectors[14–16] and flexible devices[17]. Moreover, researchers have shown their keen interest in observing photoresponse in MoS_2 based photovoltaic and optoelectronic devices[18–20]. The first optoelectronic device based on monolayer MoS_2 was a phototransistor with photoresponsivity of 7.5 mA/W fabricated by Yin *et al.*[19]. High photoresponsivity of 880 A/W much higher than first graphene photodetector[21] (0.5 mA/W) was achieved on mechanically exfoliated monolayer MoS_2 based photodetector[14]. Multilayer MoS_2 has also been considered in optically active devices for example, Kim *et al.* explored the optoelectronic properties of TFTs based on multilayer MoS_2 and showed that it can be used in high detectivity phototransistors[22].

Absence of dangling bonds in 2D layered materials facilitates their integration with three dimensional semiconductors to form van der Waals heterostructures. To further explore the properties of 2D layered materials for applications in nanoscale electronic and photovoltaic devices, their integration with bulk semiconductors has been explored in recent years utilizing the advantages of both 2D and 3D materials[23–31]. Heterogeneous integration of MoS_2 with bulk materials such as Si, GaN[32], SiC[33] and SnO[34] has been studied in recent past demonstrating the promising application of 2D/3D heterostructure based devices.

Considering MoS_2/GaN heterojunction, GaN being a wide bandgap semiconductor faces challenges in p-type doping. Integration of narrow bandgap semiconductors with GaN can lead to high performance devices but their performance gets limited due to lattice mismatch issue. This constraint can be solved by use of TMDCs such as MoS_2. In addition to it, heterojunction of MoS_2 and GaN can be a potential candidate in heterojunction bipolar transistor device. One of the important consequence of MoS_2/GaN heterojunction is the enhancement in the photoresponse. Wide bandgap materials such as GaN are used in UV photodetection whereas MoS_2 can show

Department of Physics, Indian Institute of Technology Delhi, New Delhi, 110016, India. Correspondence and requests for materials should be addressed to M.M. (email: monikamoun18@gmail.com)

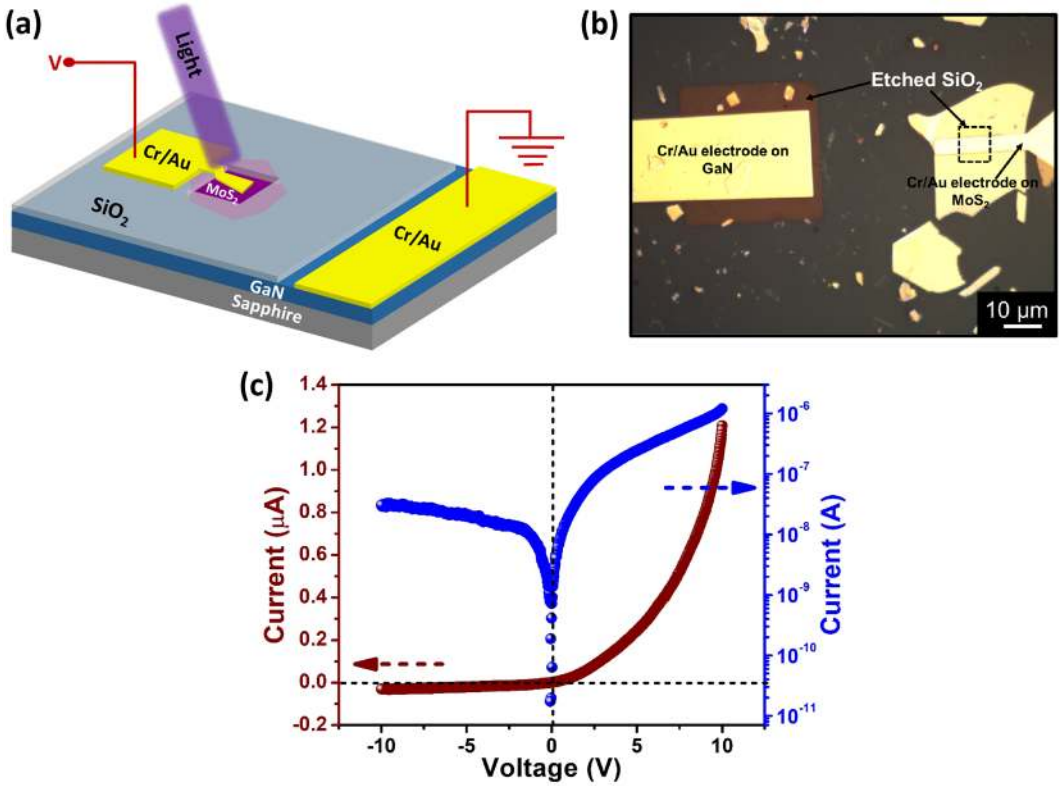

Figure 1. (**a**) 3D Schematic illustration of MoS_2/GaN heterojunction device. (**b**) Optical microscope image of the fabricated heterojunction with Cr/Au (5 nm/50 nm) contacts. (**c**) Two terminal electrical measurements of the MoS_2/GaN heterojunction diode under dark conditions showing clear current rectification.

response varying from visible to near infrared region since its bandgap lies in the range 1–2 eV. Thus, broadband photodetection can be achieved by integrating GaN with MoS_2.

In the recent years, a few reports have investigated MoS_2/GaN heterojunction as a promising platform for electronic devices[35–37]. Duan *et al*. reported strong enhancement of electroluminescence in vertically stacked MoS_2/GaN heterostructure which is difficult to achieve in other traditional indirect bandgap semiconductors[36]. Semiconductor-insulator-semiconductor diode consisting of MoS_2, h-BN and GaN has been demonstrated by Jeong *et al*. exhibiting diode like characteristics and photoresponsivity of 1.2 mA/W[37]. These investigations demonstrated that MoS_2/GaN heterojunctions have great potential in high performance electronic devices.

In the present work, fabrication of exfoliated MoS_2/GaN heterojunction and its characterization using KPFM and current-voltage (I-V) measurements have been reported. Determination of parameters such as work function difference and conduction band offset play important role to understand the charge transport in 2D/3D heterojunction. We focus on understanding of type II band alignment at the interface of MoS_2/GaN heterojunction. Further, we emphasize on understanding photoresponse behavior of the heterojunction and show that heterojunction of multilayer MoS_2 with GaN can be used in optoelectronic applications. Detailed investigation of band offset and high photoresponsivity of MoS_2/GaN heterojunction can open a pathway for the integration of dissimilar semiconductors. This may lead to high performance, energy efficient optoelectronic devices, also their incorporation can enhance the functionality of both wide band gap semiconductors and 2D layered semiconductors.

Results

The most common method for growth of MoS_2 in the fabrication of 2D/3D heterostructures is the chemical method whereas mechanically exfoliated MoS_2 is reported to have excellent crystalline nature with less defects and can offer excellent device properties as compared to chemically synthesized MoS_2. The presence of MoS_2 flakes exfoliated from bulk crystal onto GaN substrate was confirmed using Raman spectroscopy and thickness was measured using AFM (shown in supporting Fig. S1). The dominant modes of vibrations which are usually observed in Raman spectra are $E_{2g}{}^1$ and A_{1g} indicating in plane and out of plane vibrations, respectively. The $E_{2g}{}^1$ and A_{1g} modes are located at 383.8 cm^{-1} and 408.3 cm^{-1}, respectively. The difference between the Raman peaks is measured to be 24.5 cm^{-1} which indicates the existence of multilayer MoS_2[38].

Electrical characterization of exfoliated MoS_2/n-GaN heterojunction. To evaluate the electrical performance of the heterojunction, I-V measurements at room temperature were carried out. Before fabrication of the heterojunction, ohmic contacts on MoS_2 and GaN were studied separately. Cr/Au was chosen as ohmic contact on GaN as well as on MoS_2 (Supporting Information, Figs S2 and S3). 3D schematic diagram of the fabricated device and the optical image of the device are shown in Fig. 1(a,b). The current-voltage characteristics of the

MoS_2/GaN heterojunction under dark is shown in Fig. 1c. The I-V curve exhibits diode like rectifying behavior. Nearly ohmic behavior of Cr/Au contact to MoS_2 as well as on GaN proves that the diode like characteristic stems from MoS_2/GaN heterojunction.

MoS_2 is considered to be n-type semiconductor intrinsically[39]. The n-MoS_2/n-GaN heterojunction can be considered similar to metal-semiconductor contact and carrier transport is mainly due to majority charge carriers[40]. Since the current transport is dominated by only one type of carriers i.e. electrons similar to Schottky barrier diode, thermionic emission current equation can be applied. Therefore, barrier height and ideality factor can be calculated by slope and intercept of semi-log I-V curve:

$$I = A\ .\ A^{*}T^{2}\exp\left(\frac{-e\phi}{kT}\right) \times \left[\exp\left(\frac{eV}{\eta kT}\right) - 1\right] \tag{1}$$

where A is the effective area of the device ~60 μm^2. The parameter $A^{*} = 4\pi em^{*}k^2/h^3$ is the effective Richardson constant where m* is the charge carrier's effective mass (0.57 m_o for MoS_2)[41], h and k are Planck's constant and Boltzmann constant, respectively. ϕ is the barrier height and η is the ideality factor.

Barrier height and ideality factor can be further calculated using following equations:

$$\phi = \frac{kT}{e}\ ln\left(\frac{AA^{*}T^{2}}{I_s}\right) \tag{2}$$

where $I_s = A\ .\ A^{*}T^{2}\exp\left(\frac{-e\phi}{kT}\right)$ is the saturation current

$$\eta = \frac{q}{kT\left\{\frac{d(\ln I)}{dV}\right\}} \tag{3}$$

Based on the above equations, barrier height and ideality factor are estimated to be 0.50 eV and 11, respectively. Very large ideality factor (~38) is reported earlier in case of MoS_2/GaN heterojunction as measured by CAFM[35]. The unusual large value of ideality factor is due to the interface states. Since the heterojunction diode is fabricated using scotch tape method, interface between MoS_2 and GaN is not devoid of these interface states. Therefore, the current transport mechanism will deviate significantly from thermionic emission and other transport processes such as tunneling and recombination become dominantly, thus increasing the value of ideality factor.

Photoresponse properties of the heterojunction. Photoresponse properties of heterojunction are investigated by irradiating the device with 405 nm laser (Energy: 3.1 eV, greater than the MoS_2 bandgap and lower than the bandgap of GaN). To explore the photoexcitation at the heterojunction, the photoresponse of the device was investigated with varying laser intensity ranging from 0.02 mW/cm^2 to 16.6 mW/cm^2 as illustrated in Fig. 2(a). Current was observed to enhance on irradiating light. At a bias of 5 V, current enhances from 2.43×10^{-7} A to 4.53×10^{-5} A at illumination intensity of 12 mW/cm^2 giving on/off ratio of about 186.

Moreover, figure of merit parameters such as responsivity and detectivity were evaluated to check the performance of the device. Efficiency of a detector to respond to the incident light is indicated by photoresponsivity given by:

$$\mathrm{R} = \frac{\mathrm{I_{illuminated}} - \mathrm{I_{dark}}}{\mathrm{P_{illuminated}}} \tag{4}$$

where $I_{illuminated}$, I_{dark} and $P_{illuminated}$ are the current after illumination, dark current and illuminated power of laser light falling on the active area of the device, respectively[42]. Detectivity is also a critical parameter representing ability of detector to detect low optical signals and it can be estimated by[22]

$$\mathrm{D} = \frac{\mathrm{R}\ .\ \mathrm{A}^{1/2}}{\sqrt{2\mathrm{eI_d}}} \tag{5}$$

where R is the responsivity, I_d is the dark current which is 0.2 μA at biasing of 5 V, A is the area of the device where effective absorption of incident light occurs (~60 μm^2) and e is the electronic charge. The corresponding change in photoresponsivity and detectivity with illuminated power is illustrated in Fig. 2b. Decrease in both responsivity and detectivity is noted with increase in power density. The decrease in responsivity and detectivity upon increasing the power density may be attributed to the trap states present at the interface of the heterojunction[31]. Maximum responsivity and detectivity are found to be 2×10^5 A/W and 6×10^{14} jones (1 Jone = cm-Hz$^{1/2}$/W) at power density of 0.02 mW/cm^2 at the bias voltage of 5 V. Ultra high photoresponsivity and detectivity were observed at low intensity indicating that as fabricated device is highly sensitive to low incident optical power. Significant enhancement in detectivity is observed for the MoS_2/GaN heterojunction; of the order of 10^{14} Jones at 0.02 mW/cm^2 and it is higher than the value of detectivity observed in other photodetectors based on MoS_2/3D heterojunctions. The comparative study of photodetection parameters of our fabricated device with the literature is summarized in Table 1. Also, Noise-equivalent power is given by $\sqrt{2eI_d}$ and for the fabricated MoS_2/GaN heterojunction, it comes out to be 2.79×10^{-13} AHz$^{-1/2}$. Moreover, the photoresponse characteristics of the heterojunction were measured with different wavelengths (650 nm and 365 nm) (Fig. 2c,d). The heterojunction also responds to 650 nm wavelength and photoelectrical characterization reveal the high sensitivity of the fabricated

Device	Measurement parameters	Responsivity	Detectivity	Reference
MoS_2/GaN	λ = 405 nm, V = 5 V	10^5 A/W	10^{14} Jones	This work
Monolayer MoS_2 photodetector	λ = 561 nm, V = 8 V	880 A/W	—	[14]
MoS_2/Si heterojunction	λ = 808 nm, V = 0 V	300 mA/W	10^{13} Jones	[29]
MoS_2/Si heterojunction	λ = 650 nm, V = −2V	11.9 A/W	2.1×10^{10} Jones	[31]
MoS_2/hBN/GaN	Visible source, λ = 400–700 nm, V = 9 V	1.2 mA/W	—	[37]

Table 1. Performance comparison of our MoS_2/GaN heterojunction based photodetector with other MoS_2 based photodetectors.

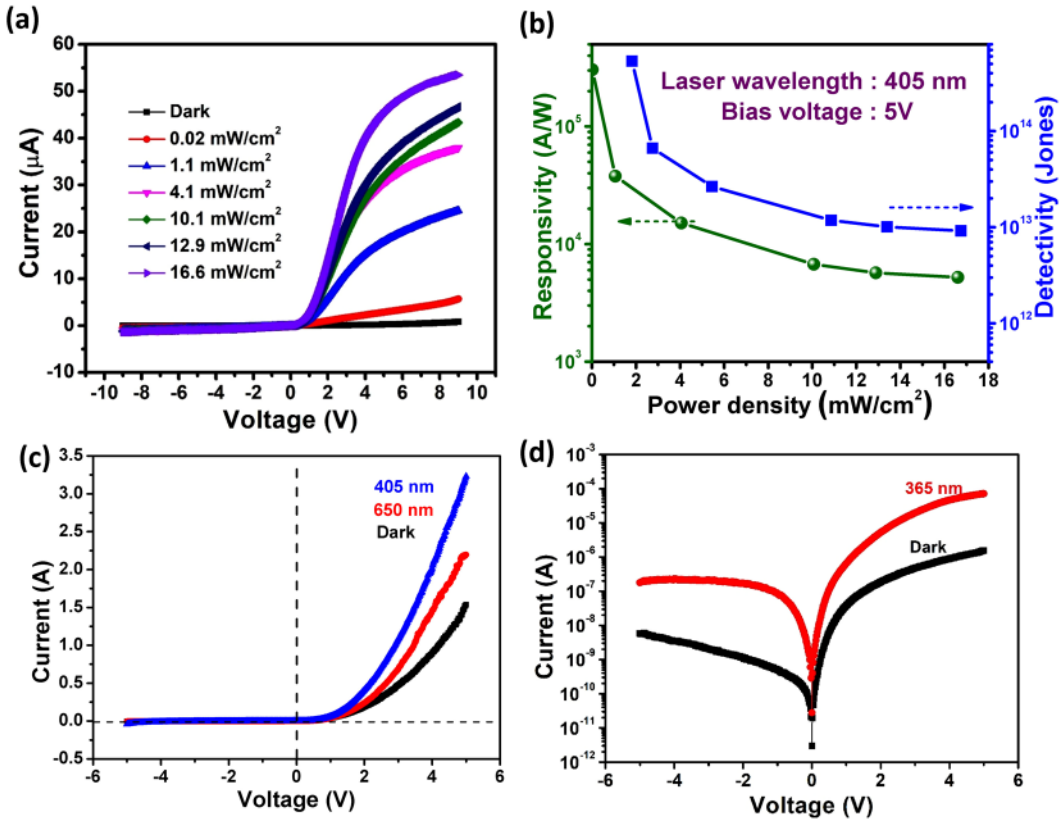

Figure 2. Photoresponse of MoS_2/GaN heterojunction under illumination with 405 nm laser. (**a**) Linear plot of photoinduced behavior of MoS_2/GaN heterojunction under different illumination intensities of 405 nm laser source. (**b**) Plots of responsivity and detectivity with light intensity. (**c**) Photoelectrical behavior of device under illumination of 650 nm and 405 nm laser. (**d**) log plot of electrical behavior of the device after exposure to UV light (365 nm).

device in UV region (365 nm). The results give a good indication that as fabricated device is showing better switching behavior and it has potential application for photodetection.

In addition, the time dependence photoresponse was investigated. Current was measured with laser on and off periodically at a constant bias of 5 V and illuminated power of 12 mW/cm^2. Photocurrent increased when laser was turned on and it decayed on turning off the laser source (Fig. 3a). The magnified plot of the response cycle is represented in Fig. 3b. An immediate drop in current was observed followed by a slow decay. The first rise and decay time of the photocurrent were measured to be 105.6 ms and 84.1 ms, respectively (Fig. 3c,d). Fast decay is due to charge carrier relaxation due to recombination and slow decay time may be attributed to trap states present at the interface of the heterojunction.

Gain is the critical parameter in photoconduction depending on ratio of carrier lifetime to transit time. Gain of the fabricated device can be expressed as:

$$G = \frac{Rh\nu}{\eta q} \tag{6}$$

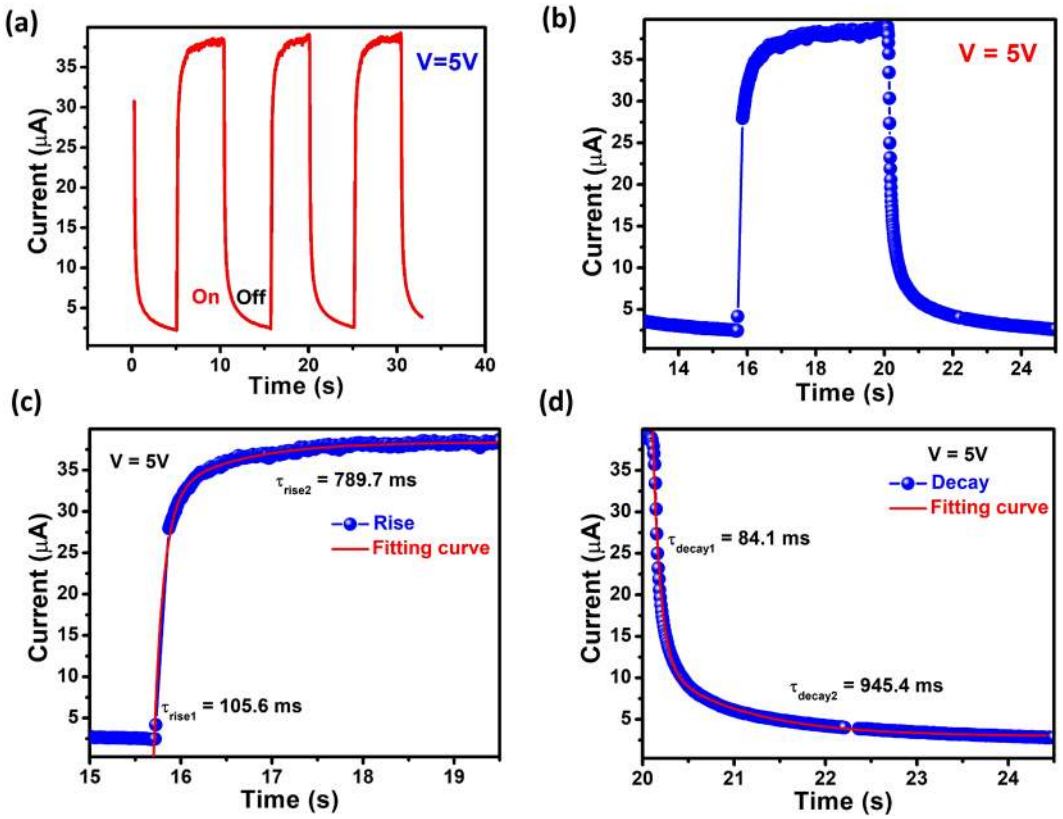

Figure 3. (**a**) Time dependence of photocurrent of the MoS_2/GaN heterojunction observed by illumination via laser light (405 nm) at a bias of 5 V with fixed illumination intensity of 12 mW/cm^2. (**b**) Magnified plot of one response cycle. (**c**) Exponential curve fitting of the rise showing fast rise time and slow rise time. (**d**) Exponential curve fitting of the decay showing fast decay time followed by slow decay (On and off represents the status when laser is on and off, respectively).

where R is the photoresponsivity, ν is the frequency of the incident light, q is the electronic charge and η is the external quantum efficiency[18]. Assuming ideal quantum efficiency to be 100%, Gain can be estimated to be 6.6×10^5 at power density of 0.02 mW/cm^2.

KPFM investigation to understand the band alignment. In order to examine the band alignment at the MoS_2/GaN interface, KPFM measurements were carried out as shown in Fig. 4(a,b). KPFM is a powerful technique used for surface potential mapping. KPFM has been previously employed to study the layer dependent work function of MoS_2[43,44] and the band alignment at 2D/3D interface[28,35]. Different methods have been employed to determine the conduction band offset of heterojunction of 2D materials with GaN[45–47]. The present investigation involves KPFM for measurement of conduction band offset. Here we experimentally investigate the change in surface potential of MoS_2 and GaN at MoS_2/GaN interface. Contact potential difference between the tip and the sample is given by:

$$(\mathrm{CPD})_{\mathrm{MoS_2}} = \frac{\phi_{\mathrm{tip}} - \phi_{\mathrm{MoS_2}}}{-e} \text{ and } (\mathrm{CPD})_{\mathrm{GaN}} = \frac{\phi_{\mathrm{tip}} - \phi_{\mathrm{GaN}}}{-e}$$

where ϕ_{tip}, ϕ_{GaN} and $\phi_{\mathrm{MoS_2}}$ are the work functions of the tip, GaN and MoS_2, respectively.

The change in contact potential difference between MoS_2 and GaN is given by:

$$\Delta\mathrm{CPD} = (\mathrm{CPD})_{\mathrm{GaN}} - (\mathrm{CPD})_{\mathrm{MoS_2}} = \frac{\phi_{\mathrm{MoS_2}} - \phi_{\mathrm{GaN}}}{-e} \sim 100\,\mathrm{mV}$$

The change in surface potential of MoS_2 and GaN is shown in Fig. 4b. The Surface potential of GaN substrate is 100 mV higher than that of the MoS_2 flake. Hence, work function difference between GaN and MoS_2 is extracted as

$$\phi_{\mathrm{GaN}} - \phi_{\mathrm{MoS_2}} \sim 100 \text{ meV}$$

Work function of GaN is observed to be greater than that of MoS_2 with a difference of about 100 meV. In this aspect, the KPFM result gives direct evidence for junction formation between MoS_2 and GaN substrate. Since for

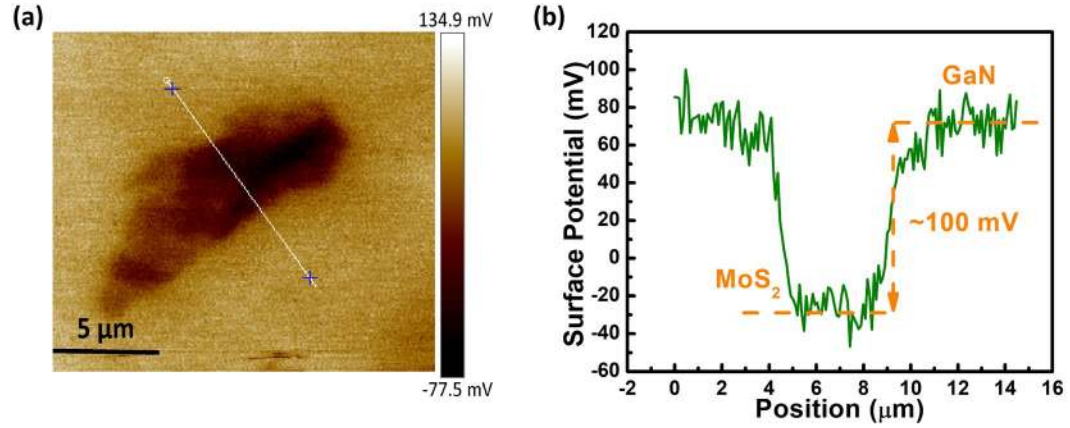

Figure 4. (**a**) Kelvin Probe Force Microscope (KPFM) image of MoS_2 flake on n-GaN showing change in surface potential between MoS_2 and GaN. (**b**) Plot of surface potential difference with lateral distance across MoS_2/GaN interface along the line as indicated in (**a**).

n-type semiconductor, relation between bottom of conduction band and fermi level is expressed as $E_C - E_F = kT\ln\left(\frac{N_C}{N_D}\right)$, therefore Conduction band offset can be further obtained by using the following equation:

$$\phi_{GaN} - \phi_{MoS_2} = \left[\Delta E_c + kT\left\{\ln\frac{\left(\frac{N_{C,GaN}}{N_{D,GaN}}\right)}{\left(\frac{N_{C,MoS_2}}{N_{D,MoS_2}}\right)}\right\}\right] \tag{7}$$

where N_D, N_C and ΔE_C are the doping density, effective density of states and conduction band offset respectively. Doping density in n-GaN is 4.6×10^{17} as measured by Hall measurement technique and doping density in MoS_2 is taken to be $10^{16}\,cm^{-3}$ [48]

Equation (7) becomes

$$\Delta E_c = \left[\left(\phi_{GaN} - \phi_{MoS_2}\right) - kT\left\{\ln\frac{\left(\frac{(m^*_{GaN})^{3/2}}{N_{D,GaN}}\right)}{\left(\frac{(m^*_{MoS_2})^{3/2}}{N_{D,MoS_2}}\right)}\right\}\right] \tag{8}$$

Effective mass values for MoS_2 and GaN are taken to be 0.57 m_o and 0.22 m_o, respectively[41,49]. Using Equation (8), conduction band offset $\Delta E_c = 0.23$ eV was estimated. According to Anderson's rule, conduction band offset depicts the difference between electron affinities of MoS_2 and GaN. It is evident from KPFM result that a junction barrier having value 0.23 eV exists between MoS_2 and GaN substrate.

On the basis of these values, built in potential (V_{bi}) and depletion width are calculated and therefore energy band diagram can be drawn to evolve the carrier transport.

Ideally, built in potential barrier is the difference between work functions of the semiconductors.

$$eV_{bi} = \phi_{GaN} - \phi_{MoS_2} = 100\,\text{meV as measured using KPFM}$$

Depletion width is given by

$$x_n = \left\{\frac{2\varepsilon_n\varepsilon_N N_{dN} V_{bi}}{eN_{dn}(\varepsilon_n N_{dn} + \varepsilon_N N_{dN})}\right\}^{1/2} \quad \text{and} \quad x_N = \left\{\frac{2\varepsilon_n\varepsilon_N N_{dn} V_{bi}}{eN_{dN}(\varepsilon_n N_{dn} + \varepsilon_N N_{dN})}\right\}^{1/2}$$

where n and N denotes MoS_2 and GaN, respectively. ε_n, ε_N, N_{dn} and N_{dN} denotes the dielectric constant of MoS_2, dielectric constant of GaN, doping density in MoS_2 ($10^{16}\,cm^{-3}$) and GaN ($4.6 \times 10^{17}\,cm^{-3}$), respectively. Using above values, depletion width in MoS_2 and GaN is calculated to be 104 nm and 2.26 nm, respectively.

Furthermore, built in potential barrier in both the regions can be calculated using following equation:

$$V_{bi} = V_{bin} + V_{biN} = \frac{eN_{dn}x_n^{\,2}}{2\varepsilon_n} + \frac{eN_{dN}x_N^{\,2}}{2\varepsilon_N}$$
$$V_{bin} = 97\,\text{mV and } V_{bin} = 2.23\,\text{mV} \tag{9}$$

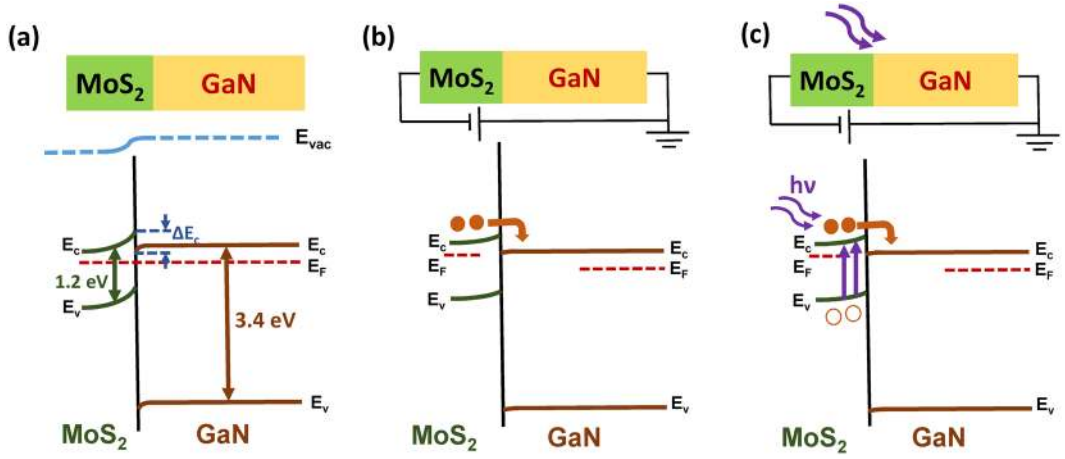

Figure 5. Energy band diagram of the heterojunction. (**a**) After contact (zero bias). (**b**) Forward bias (negative bias is given to MoS_2 with respect to GaN). (**c**) Forward bias under photoexcitation with laser wavelength 405 nm. E_c, E_v, E_F and E_{vac} represent bottom of conduction band, top of valence band, Fermi level and vacuum level, respectively. Band gap of MoS_2 and GaN is 1.2 eV and 3.4 eV, respectively. ΔE_c represents the conduction band offset.

Built in potential barrier in MoS_2 and GaN region are calculated to be 97 mV and 2.23 mV, respectively. The calculated values of depletion width and built-in potential barrier in both the regions help in evolving the band diagram and the charge transport.

Discussion

In order to understand the carrier transport and photoresponse of the device, a possible mechanism is proposed based on type II band alignment as illustrated in Fig. 5(a–c). Band diagram is drawn based on the above calculated parameters based on KPFM such as built in potential, depletion width and conduction band offset. Figure 5a represents the schematic of the band alignment under zero bias condition demonstrating type- II heterojunction. Under equilibrium condition, when MoS_2 is in contact with GaN, band bending occurs in order to align the Fermi level. Since Fermi level of MoS_2 is at higher energy level than that of GaN, electrons in MoS_2 side will tend to move to GaN forming a built in potential at the interface. MoS_2 acquires a depletion region whereas GaN acquires an accumulation region near the interface. Depletion width and built in potential in MoS_2 region is larger than that of GaN region as calculated above. When MoS_2 is given negative voltage with respect to GaN, higher current is observed compared to reverse bias case. Schematic of energy band structure on biasing is illustrated in Fig. 5b. When MoS_2 is forward biased with respect to GaN, band edge of MoS_2 raises and that of GaN lowers down. Electrons from MoS_2 region can transport to GaN region due to decrease of effective barrier for flow of electrons from left side to right side giving high value of current. However, when MoS_2 is reverse biased with respect to GaN, there is less probability for electrons in MoS_2 region to move to GaN region because of relatively higher barrier. Hole current is not considered due to essential lack of holes.

Under illumination with light energy (405 nm) higher than bandgap of MoS_2, electron hole pairs are generated preferentially in MoS_2 due to lower incident excitation energy than bandgap of GaN as shown in Fig. 5c. When negative voltage is applied to MoS_2, photocurrent is enhanced due to transport of photogenerated electrons from MoS_2 region to GaN region. The observed lesser current in reverse biased case is due to higher barrier formation for photogenerated carriers to flow from MoS_2 to GaN. However, when the device is illuminated with 365 nm laser, large photocurrent is observed. Electrodes on MoS_2 and GaN are separated by a distance of nearly 60 μm whereas spot size of the incident laser is 2 mm. The incident light is illuminating both GaN and MoS_2. Since 365 nm wavelength is corresponding to bandgap of GaN, electron-hole pairs are generated in GaN also leading to significant enhancement in current. Both MoS_2 and GaN are contributing to the total current leading to large enhancement in the photocurrent.

Conclusions

MoS_2/GaN diode which is a type-II heterojunction has been fabricated. The type II band alignment of 2D MoS_2/GaN heterojunction has been investigated by measuring change in surface potential and corresponding change in work functions of MoS_2 and GaN. The conduction band offset of 0.23 eV was extracted using KPFM. From the current-voltage measurements, the heterojunction exhibited diode like behavior with barrier height of 0.50 eV in dark. In addition, the photoresponse behavior of the device was explored and the device was highly sensitive to 405 nm laser. The as fabricated heterojunction exhibited excellent optoelectronic performance such as ultrahigh photoresponsivity as 10^5 A/W, gain as 10^5 and detectivity of the order of 10^{14} Jones. These results show that 2D MoS_2/GaN can be used in efficient photodetection applications. Our results can pave the way in designing the optoelectronic devices based on integration of low dimensional materials with conventional 3D semiconductors.

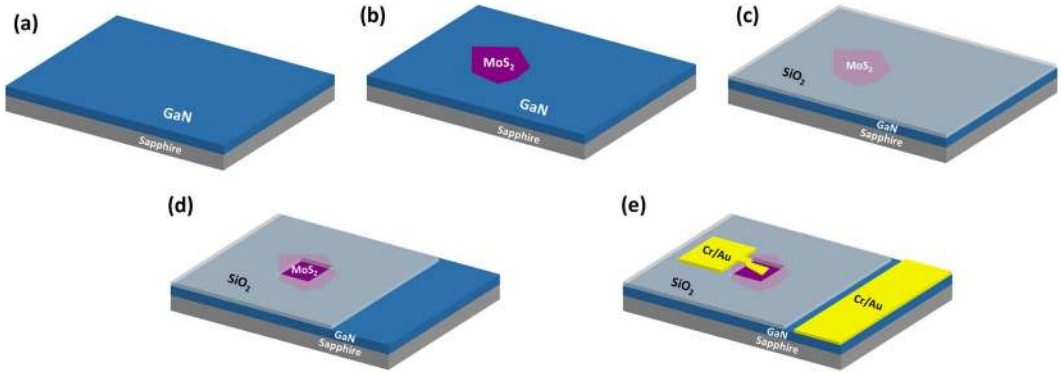

Figure 6. Process flow of the fabrication process. (**a**) GaN/Sapphire substrate. (**b**) Transfer of MoS_2 flakes on GaN/Sapphire substrate. (**c**) Deposition of SiO_2 on the template for insulation of electrodes. (**d**) Selective etching of SiO_2 over MoS_2 and GaN. (**e**) Electrode deposition on MoS_2 and GaN.

Experimental Section

The MOVPE grown Gallium Nitride (GaN) epitaxial film on c-plane sapphire substrate with 3 μm thickness has been used for MoS_2/GaN heterojunction. The GaN layer exhibits n-type behavior, sheet resistance of about 285 Ω/square, carrier concentration of 4.6×10^{17} cm^{-3} and Hall electron mobility of about 160 cm^2/Vs at room temperature, as measured by Ecopia Hall measurement set up (HMS 5000). The samples were ultrasonically cleaned in acetone followed by iso-propanol and De-ionized water (DI-Water) for 5 minutes each, to remove the organic contaminants. In order to etch the native oxide layer from the surface, samples were dipped in the solution of HCl: H_2O in the ratio of 1:2 for 30 s. Samples were again rinsed with DI water and thereafter dried with nitrogen gun.

MoS_2 crystal was purchased from SPI supplies. For the fabrication of MoS_2-GaN heterojunction, 2D MoS_2 flakes were transferred on GaN/sapphire from MoS_2 crystal using mechanical exfoliation method (Fig. 6a,b). Raman measurement was conducted to confirm the MoS_2 flake using micro- Raman system (Horiba LabRAM HR evolution) with laser excitation wavelength of 514 nm. KPFM measurements were performed using Bruker multi mode Atomic Force Microscope in tapping mode. Pt coated Si tip was used to scan the samples and samples were grounded during the measurements.

After transfer of MoS_2 on GaN, SiO_2 of thickness 100 nm was deposited on MoS_2/GaN sample using sputtering as an insulating layer (Fig. 6c). PMMA resist was spin coated on the template. Windows were opened on top of MoS_2 (8 μm × 8 μm) and GaN (40 μm × 40 μm) using Electron beam lithography (Model No: eLine plus from Raith GmbH). SiO_2 was etched away within the opened window by dipping the sample in 10% HF for 10 seconds (Fig. 6d). After removing the remaining resist in acetone, again electron beam lithography was used to pattern the electrodes over MoS_2 and GaN. Finally, metal contacts were deposited using sputtering system followed by lift off of resist in acetone. Cr/Au (5 nm/50 nm) was chosen as top electrode on MoS_2 as well as bottom electrode on GaN (Fig. 6e). Current-voltage characteristics of the device were measured using DC probe station (EverBeing-EB6) and Semiconductor Characterization System (Keithley: SCS-4200) under dark and illuminated conditions. Tungsten tips were used to probe the electrodes. For illumination of the device, laser source was used. Photoresponse of the device was measured at different power densities of the light.

References

1. Wang, Q. H., Kalantar-Zadeh, K., Kis, A., Coleman, J. N. & Strano, M. S. Electronics and optoelectronics of two-dimensional transition metal dichalcogenides. *Nature nanotechnology* **7**, 699–712 (2012).
2. Lee, C. H. *et al.* Atomically thin p-n junctions with van der Waals heterointerfaces. *Nature nanotechnology* **9**, 676–681 (2014).
3. Lopez-Sanchez, O. *et al.* Light Generation and Harvesting in a van der Waals Heterostructure. *Acs Nano* **8**, 3042–3048 (2014).
4. Cheiwchanchamnangij, T. & Lambrecht, W. R. L. Quasiparticle band structure calculation of monolayer, bilayer, and bulk MoS_2. *Phys Rev B* **85**, 205302 (2012).
5. Lebegue, S. & Eriksson, O. Electronic structure of two-dimensional crystals from ab initio theory. *Phys Rev B* **79**, 115409 (2009).
6. Bernardi, M., Palummo, M. & Grossman, J. C. Extraordinary Sunlight Absorption and One Nanometer Thick Photovoltaics Using Two-Dimensional Monolayer Materials. *Nano letters* **13**, 3664–3670 (2013).
7. Eda, G. & Maier, S. A. Two-Dimensional Crystals: Managing Light for Optoelectronics. *Acs Nano* **7**, 5660–5665 (2013).
8. Hu, G. H. *et al.* Black phosphorus ink formulation for inkjet printing of optoelectronics and photonics. *Nat Commun* **8**, 278 (2017).
9. Mak, K. F., Lee, C., Hone, J., Shan, J. & Heinz, T. F. Atomically Thin MoS_2: A New Direct-Gap Semiconductor. *Phys Rev Lett* **105**, 136805 (2010).
10. Kwak, J. Y. *et al.* Electrical Characteristics of Multilayer MoS_2 FET's with MoS2/Graphene Heterojunction Contacts. *Nano letters* **14**, 4511–4516 (2014).
11. Li, H. *et al.* Fabrication of Single- and Multilayer MoS_2 Film-Based Field-Effect Transistors for Sensing NO at Room Temperature. *Small* **8**, 63–67 (2012).
12. He, Q. Y. *et al.* Fabrication of Flexible MoS_2 Thin-Film Transistor Arrays for Practical Gas-Sensing Applications. *Small* **8**, 2994–2999 (2012).
13. Late, D. J. *et al.* Sensing Behavior of Atomically Thin-Layered MoS_2 Transistors. *Acs Nano* **7**, 4879–4891 (2013).
14. Lopez-Sanchez, O., Lembke, D., Kayci, M., Radenovic, A. & Kis, A. Ultrasensitive photodetectors based on monolayer MoS_2. *Nature nanotechnology* **8**, 497–501 (2013).
15. Kufer, D. & Konstantatos, G. Highly Sensitive, Encapsulated MoS_2 Photodetector with Gate Controllable Gain and Speed. *Nano letters* **15**, 7307–7313 (2015).

16. Wang, X. D. *et al*. Ultrasensitive and Broadband MoS_2 Photodetector Driven by Ferroelectrics. *Advanced materials* **27**, 6575–6581 (2015).
17. Salvatore, G. A. *et al*. Fabrication and Transfer of Flexible Few-Layers MoS_2 Thin Film Transistors to Any Arbitrary Substrate. *Acs Nano* **7**, 8809–8815 (2013).
18. Zhang, W. *et al*. High-gain phototransistors based on a CVD MoS_2 monolayer. *Advanced materials* **25**, 3456–3461 (2013).
19. Yin, Z. Y. *et al*. Single-Layer MoS_2 Phototransistors. *Acs Nano* **6**, 74–80 (2012).
20. Lee, H. S. *et al*. MoS_2 Nanosheet Phototransistors with Thickness-Modulated Optical Energy Gap. *Nano letters* **12**, 3695–3700 (2012).
21. Xia, F. N., Mueller, T., Lin, Y. M., Valdes-Garcia, A. & Avouris, P. Ultrafast graphene photodetector. *Nature nanotechnology* **4**, 839–843 (2009).
22. Choi, W. *et al*. High-detectivity multilayer MoS_2 phototransistors with spectral response from ultraviolet to infrared. *Advanced materials* **24**, 5832–5836 (2012).
23. Ali, A. *et al*. High-Performance, Flexible Graphene/Ultra-thin Silicon Ultra-Violet Image Sensor. *IEEE* **17**, 203–206 (2017).
24. Chen, S. *et al*. Facile Synthesis of gamma-In_2Se_3 Nanoflowers toward High Performance Self-Powered Broadband gamma-In_2Se_3/Si Heterojunction Photodiode. *Small* **13**, 1604033 (2017).
25. Wan, X. *et al*. A self-powered high-performance graphene/silicon ultraviolet photodetector with ultra-shallow junction: breaking the limit of silicon? *npj 2D Materials and Applications* **1**, 4 (2017).
26. Xu, Y. *et al*. Solvent-Based Soft-Patterning of Graphene Lateral Heterostructures for Broadband High-Speed Metal-Semiconductor-Metal Photodetectors. *Advanced Materials Technologies* **2**, 1600241 (2017).
27. Li, B. *et al*. 3D Band Diagram and Photoexcitation of 2D-3D Semiconductor Heterojunctions. *Nano letters* **15**, 5919–5925 (2015).
28. Li, Y., Xu, C. Y., Wang, J. Y. & Zhen, L. Photodiode-Like Behavior and Excellent Photoresponse of Vertical Si/Monolayer MoS_2 Heterostructures. *Sci Rep-Uk* **4**, 7186 (2014).
29. Zhang, Y. *et al*. *In Situ* Fabrication of Vertical Multilayered MoS_2/Si Homotype Heterojunction for High-Speed Visible-Near-Infrared Photodetectors. *Small* **12**, 1062–1071 (2016).
30. Dhyani, V. & Das, S. High-Speed Scalable Silicon-MoS_2 P-N Heterojunction Photodetectors. *Sci Rep-Uk* **7**, 44243 (2017).
31. Wang, L. *et al*. MoS_2/Si Heterojunction with Vertically Standing Layered Structure for Ultrafast, High-Detectivity, Self-Driven Visible-Near Infrared Photodetectors. *Adv Funct Mater* **25**, 2910–2919 (2015).
32. Lee, E. W. *et al*. Layer-transferred MoS_2/GaN PN diodes. *Appl Phys Lett* **107**, 103505 (2015).
33. Lee, E. W. *et al*. Growth and electrical characterization of two-dimensional layered MoS_2/SiC heterojunctions. *Appl Phys Lett* **105**, 203504 (2014).
34. Wang, Z. W., He, X., Zhang, X. X. & Alshareef, H. N. Hybrid van der Waals p-n Heterojunctions based on SnO and 2D MoS_2. *Advanced materials* **28**, 9133–9144 (2016).
35. Ruzmetov, D. *et al*. Vertical 2D/3D Semiconductor Heterostructures Based on Epitaxial Molybdenum Disulfide and Gallium Nitride. *Acs Nano* **10**, 3580–3588 (2016).
36. Li, D. H. *et al*. Electric-field-induced strong enhancement of electroluminescence in multilayer molybdenum disulfide. *Nat Commun* **6**, 7509 (2015).
37. Jeong, H. *et al*. Semiconductor-Insulator-Semiconductor Diode Consisting of Monolayer MoS_2, h-BN, and GaN Heterostructure. *Acs Nano* **9**, 10032–10038 (2015).
38. Lee, C. *et al*. Anomalous Lattice Vibrations of Single- and Few-Layer MoS_2. *Acs Nano* **4**, 2695–2700 (2010).
39. Komsa, H. P. & Krasheninnikov, A. V. Native defects in bulk and monolayer MoS_2 from first principles. *Phys Rev B* **91**, 125304 (2015).
40. OLDHAM, W. G. & MILNES, A. G. n-n SEMICONDUCTOR HETEROJUNCTIONS*. *Solid-State Electronics* **6**, 121–132 (1963).
41. Tosun, M. *et al*. MoS_2 Heterojunctions by Thickness Modulation. *Sci Rep-Uk* **5**, 10990 (2015).
42. Tsai, D. S. *et al*. Few-Layer MoS_2 with High Broadband Photogain and Fast Optical Switching for Use in Harsh Environments. *Acs Nano* **7**, 3905–3911 (2013).
43. Hao, G. L. *et al*. Electrostatic properties of few-layer MoS_2 films. *Aip Adv* **3**, 042125 (2013).
44. Li, Y., Xu, C. Y. & Zhen, L. Surface potential and interlayer screening effects of few-layer MoS_2 nanoflakes. *Appl Phys Lett* **102**, 143110 (2013).
45. Tangi, M. *et al*. Determination of band offsets at GaN/single-layer MoS_2 heterojunction. *Appl Phys Lett* **109**, 032104 (2016).
46. Tangi, M. *et al*. Band Alignment at GaN/Single-Layer WSe_2Interface. *Acs Appl Mater Inter* **9**, 9110–9117 (2017).
47. Henck, H. *et al*. Interface dipole and band bending in the hybrid p-n heterojunction MoS_2/GaN(0001). *Phys Rev B* **96**, 115312 (2017).
48. Kim, S. *et al*. High-mobility and low-power thin-film transistors based on multilayer MoS_2 crystals. *Nat Commun* **3**, 1011 (2012).
49. Kumar, A., Kashid, R., Ghosh, A., Kumar, V. & Singh, R. Enhanced Thermionic Emission and Low 1/f Noise in Exfoliated Graphene/GaN Schottky Barrier Diode. *Acs Appl Mater Inter* **8**, 8213–8223 (2016).

Acknowledgements

We would like to acknowledge Nanoscale Research Facility (NRF) at Indian Institute of Technology Delhi for fabrication and characterization techniques like Electron Beam Lithography, Raman, KPFM and electrical measurements. Monika Moun would like to thank University Grants Commission (UGC), India for providing senior research fellowship (SRF).

Author Contributions

M.M. and R.S. designed the experiments. M.M. fabricated and characterized the device. R.P. contributed to KPFM measurements. M.K. and M.G. discussed the results and contributed to the manuscript preparation. M.M. compiled and wrote the manuscript which was read and approved by all the authors.

Additional Information

Supplementary information accompanies this paper at https://doi.org/10.1038/s41598-018-30237-8.

Competing Interests: The authors declare no competing interests.

Publisher's note: Springer Nature remains neutral with regard to jurisdictional claims in published maps and institutional affiliations.